Laboratoire de Physique Nucléaire et de Hautes Énergies
CNRS - IN2P3 - Universités Paris VI et VII

Testing Megacam with SNDICE

E. Barrelet, K.Schahmaneche

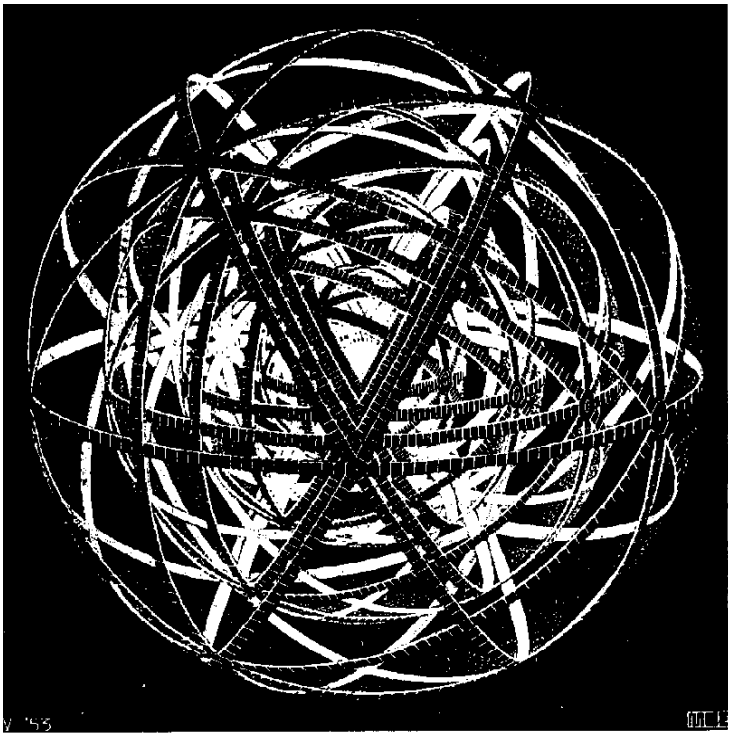

4, Place Jussieu - Tour 33 - Rez-de-Chaussée
75252 Paris Cedex 05
Tél.: 33(1) 44 27 63 13 - FAX: 33(1) 44 27 46 38

1 Introduction

We have gathered in this report the results of the tests using a sequence of Megacam images produced by SNDICE light source in a fixed position relatively to the telescope. The underlying hypothesis, knowing the great stability of SNDICE illumination (~10^{-4}), is a fixed and almost uniform distribution of light on the pixels of the 36 CCD's multiplexed through 72 amplifiers reading each arrays of 1024*4620 pixels. The first issue will therefore be to test the response of Megacam electronics to an infalling light flux on each pixel constant during a given exposure time, whether this time is fixed by the mechanical Megacam shutter or the Sndice electronic shutter. The next issue is the response of Megacam electronics to a variable and well known integrated flux. The flux can be programmed very precisely either by fixing the exposure time (electronically or mechanically) or the LED current (here again SNDICE flux is controlled at a ~10^{-4} precision).

2 Methods used for the analysis of Megacam images

2.1 Data structure

A Megacam raw data image is made of 72 ' amplifier' blocks numbered 0 to 71. The two amplifiers belonging to the same CCD are numbered by an even number followed by the next odd number. The CCD are numbered from 0 to 35 as shown in Figure 1, hence the

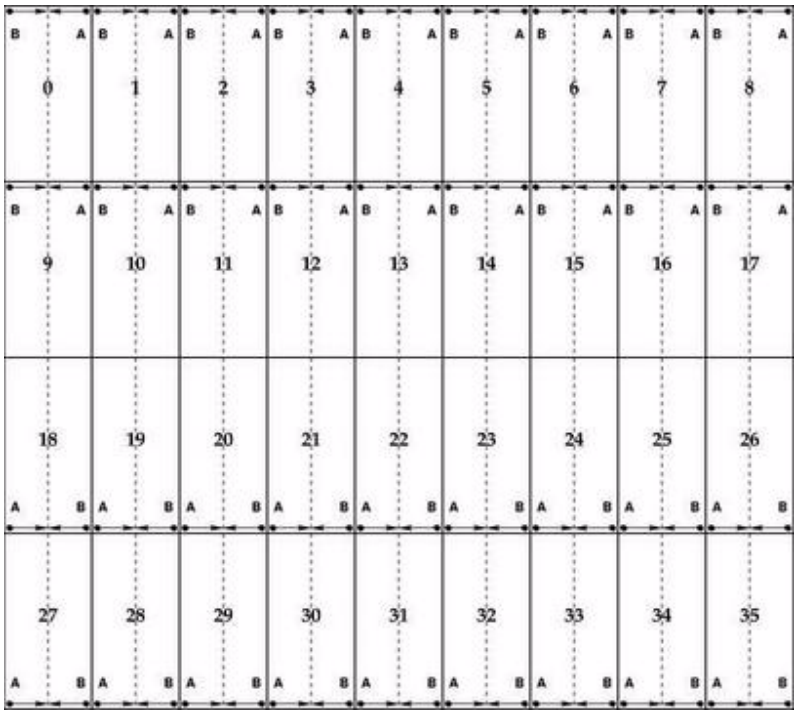

Figure 1: Megacam CCD numbering scheme (N_{CCD} =0-35). The two amplifiers A and B on each CCD are situated in a corner and the nearest pixel is read first (pixel (col=1; line=1). The amplifier number is N_{CCD}*2+0 (left amp) or N_{CCD}*2+1 (right amp).

amplifiers are numbered from 0 to 71 (or from 1 to 72). Each image block, as in Figure 2,

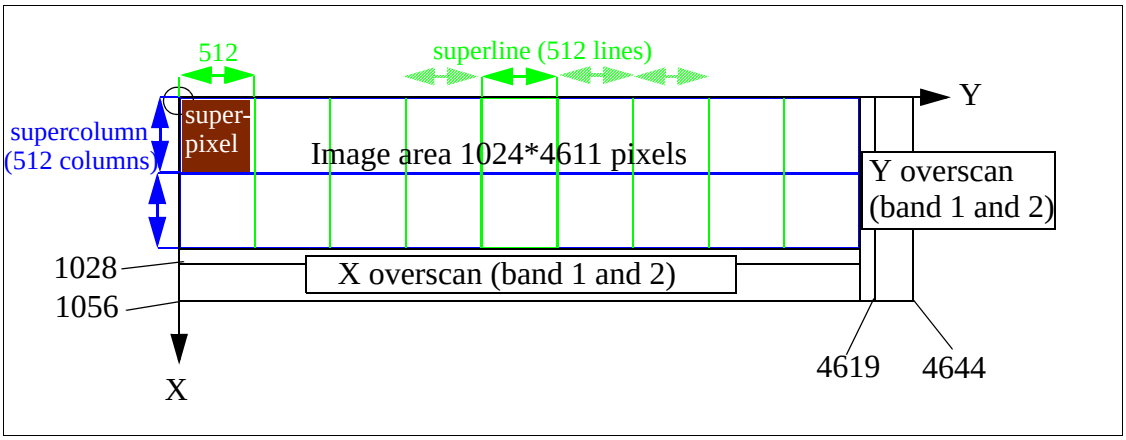

Figure 2: Organization of the pixel array corresponding to one amplifier (two amplifiers per CCD)

contains 1024*4611 real pixels and a few dummy 'overscan' pixels extending the line size to 1056 pixels (electrons traversing only the full serial register) and extending the number of lines to 4644 (electrons traversing the full image area during the image readout period). The image area will be limited to 1024*4608 pixels by suppressing the last three lines, in order to exploit a 2*9 "superpixel" structure (a superpixel block is a 512*512 pixels array). The area covered by a given amplifier is covered by two "supercolumns" or 9 "superlines".
Each overscan area is divided in two bands: band 1 contains trailing charges left over from the image and band 2 contains clean 'pedestal'.

2.2 Y overscan

Figure 3-a) shows some residual electrons trailing in the Y overscan region (in particular

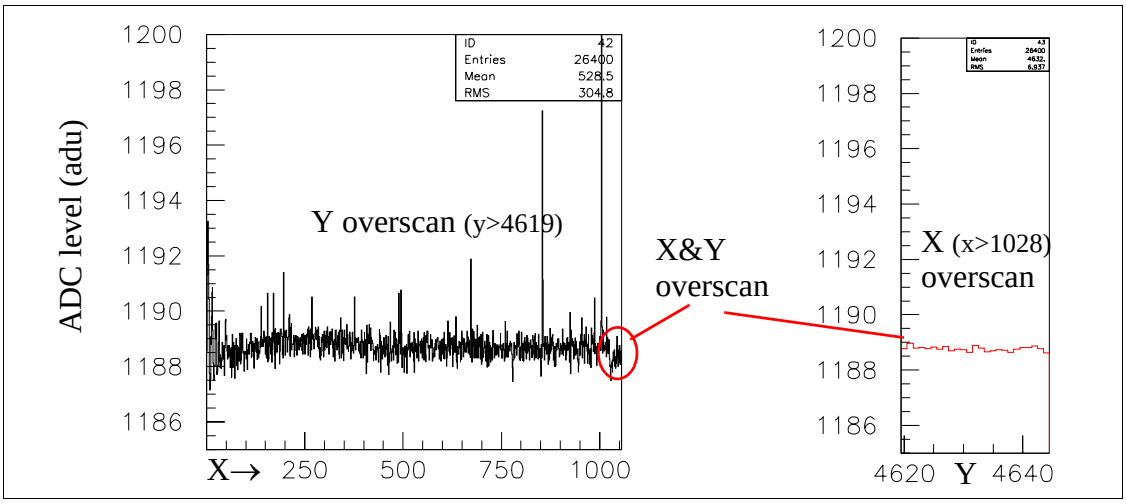

Figure 3: a) X profile of Y overscan (band 2); b) Y profile of X&Y overscan

inside a few columns which contains pixels with long lifetime traps).

The mean adc value in the double overscan region (X>1028 and Y>4619) gives the best estimate of the rest state of the electronic when the CCD is not filled nor clocked. However this does not prove that this is the common 'pedestal' value 'P' to be subtracted from each adc reading in every image to yield 'K' times the number of photoelectrons generated in the corresponding pixel.
Measuring P and K is by definition to perform the electronic calibration of the CCD camera.

2.3 X overscan

At least two effects seen in the X overscan region are conspiring to bias the pedestal value (one positive and one negative).
The first effect affecting flat field images by opposition to astronomy images is the next-serial-pixel trailing signal seen in the band 1 of X overscan (an overshoot). The second effect is an undershoot seen in Figure 4-a). The depth of this undershoot is

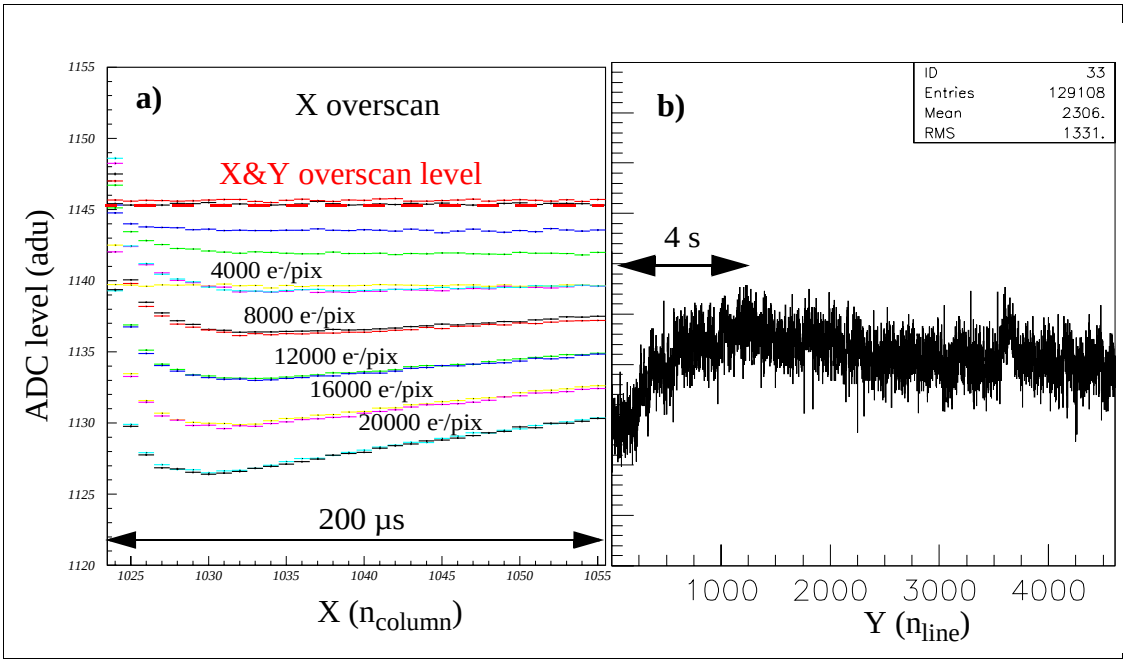

Figure 4: **a)** X profile of the X overscan region: it shows the relaxation of the pedestal level following the readout of a uniformly bright flat field images
b) Y profile of the mean X overscan region:

proportional to mean charge inside the image. It characterizes the restoration of the electronic system (e.g. the refilling of the decoupling capacitances) after reading a full line at high level. The time interval covered by the plot in Figure 4-a is around 200µs. The time left for a parallel line transfer, before reading the next line, is of the same order of magnitude. This is not enough to recover the rest level represented by a dashed red line just above the overscan of a low level image. The rise of pedestal level seen during the readout of the first 1000 lines in Figure 4-b (duration around 4s) is a much slower process. It might be thermal. The observed phenomena are not self explanatory: one

would need a detailed study of the Megacam electronics in order to model the relation between the behaviour of the overscan and the pedestal to be subtracted in the image region. Another approach is to extrapolate linearly the level of the image in each column as a function of flux to zero.

2.4 Image area

The goal of this section is to obtain a first order Sndice calibration without studying in detail the diffraction rings seen in the images. The uniformity and the reproducibility of the illumination of the focal plane and the linearity[1] of the CCD response to the sndice integrated flux is supposed. (Studying the deviations from these assumptions will be the task of Section 3).
From this point of view the main characteristic of Sndice-Megacam images shown in Figure 5 a) is the distribution of pixel intensities, approximatively gaussian with a 4%

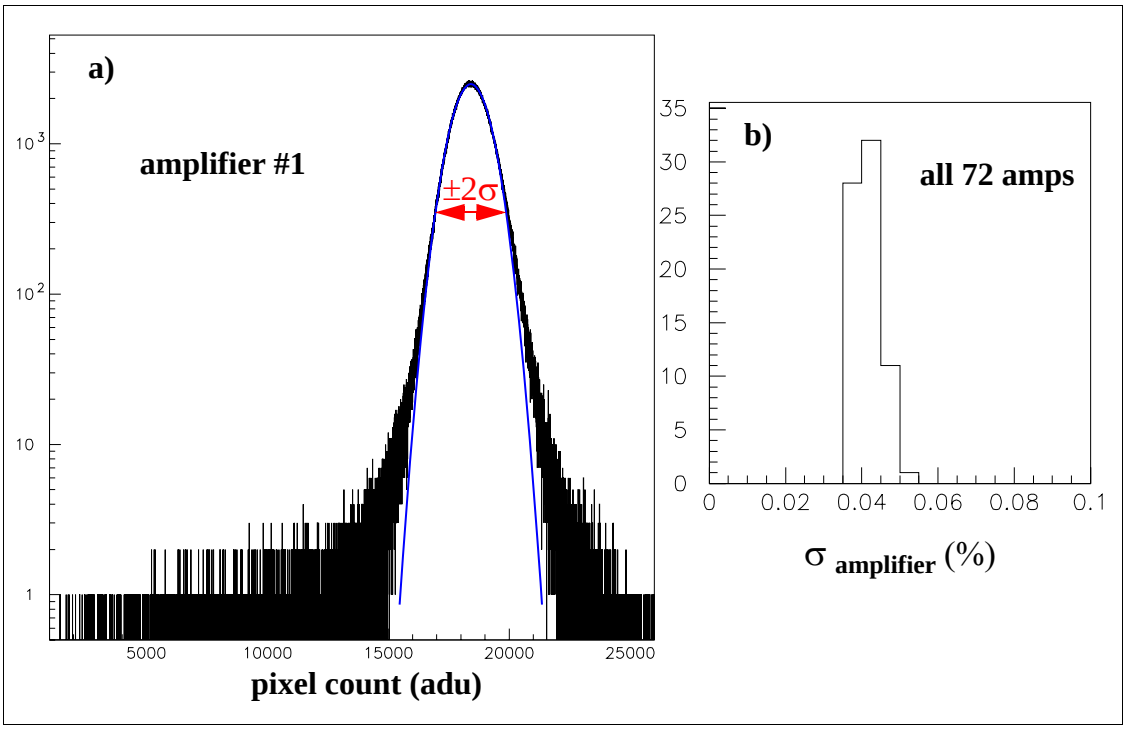

Figure 5: **a)** single pixel ADC-count for one amplifier (σ is RMS contrast by definition);
b) The distribution of RMS contrast across the megacam focal plane is rather uniformly distributed around 4%

RMS (which by definition is the RMS contrast of the image). This contrast is essentially due to diffraction rings of different amplitude and scale seen in the image, with tails of the distribution due to the sharper rings and the dark spots. Technically it could be called a 'stochastic texture'. The RMS of the photon noise ('Poisson' statistics) in a typical pixel containing $2*10^4$ e^- is a quarter of the RMS contrast. Therefore it increases the

[1] the CCD transfer function which includes quantum efficiency, charge tranfer efficiency, preamplification, amplification and digitization is supposed identical for each pixel

RMS contrast only by 3.4%.
A level-1 opto-electrical calibration can be introduced at this step by equalizing the means of the gaussian fits of Figure 5 and the pedestals of Figure 3. All 72 amplifiers will at this point have one pedestal P_i and one constant level gain K_i. The statistical precision of the fitted mean and rms parameters is a fraction of an adu for a level of 20000 adu. This means that precision will be limited by other factors. The first to take into consideration is the reproducibility of the constant calibrating flux, known by test bench study to be around 10^{-4} after taking into account the LED temperature.
This hypothesis is verified with a test which results are summarized in Figure 6:

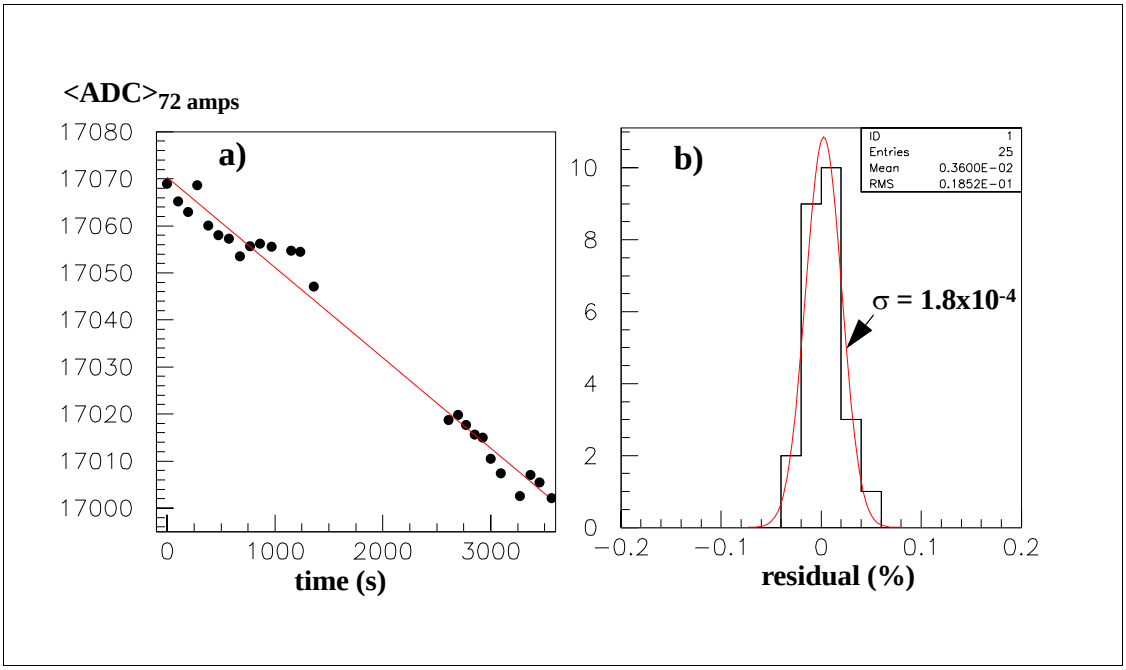

Figure 6: a) With SNDICE light pulses exposures taken during one hour, the average response of Megacam's 72 amplifiers displays a small drift. b) A linear fit of this drift yields a residual distribution with $1.8x10^{-4}$ RMS attributed to residual temperature variations.

Repeating a constant level illumination of megacam with sndice during one hour we obtained 25 images which were compared using the mean of all 72 amplifiers mean response (around 17000 adu). The drift observed in Figure 6-a is attributed to the combination of sndice and megacam electronics temperature effects (the latter is not monitored). A linear approximation of this temperature effect yields residuals within $1.8*10^{-4}$ RMS. This is in line with sndice known stability, but this means also that the not-so-good megacam stability is enhanced by the global averaging of the whole focal plane.
Another high precision feature of sndice, the possibility to ramp up the light flux very precisely and by minute steps ($0.5*10^{-4}$) can be used to study the optoelectronic response of megacam. A first try using the shutter opening time as a integrated light flux handle (also used in Figure 4-a) shows the way and the problems: one can perform a high precision regression analysis of integrated fluxes between the constant flux used for level-1 calibration and zero flux. Statistical precision is sufficient to determine the two

calibration constants of a given amplifier column per column (or line per line) and one will find that they vary! Therefore it is wiser to do this kind of high precision check of megacam electronics after studying various instabilities at constant level. This analysis has also underlined the interest of using sndice flux ramps and not shutter time ramps. The shutter time, as it is essentially a mechanical parameter, is not defined accurately enough. One finds that the megacam shutter time estimate based on a diode sensor is systematically biased.

A last opportunity resulting of the good reproducibility of sndice-megacam images is the use of the photon statistical factor to calibrate the electronic gain of each amplifier, i.e. to determine the overall gain k_e of the CCD readout chain equal to the number of adc units per electron. There are a number of ways to apply this classical method to our case. First let us have a look at the distribution of pixel by pixel differences of adc counts for two successive images of the sequence represented in Figure 6. One one hand we have a distribution for the image area in Figure 7-a perfectly fitted by a gaussian except for the

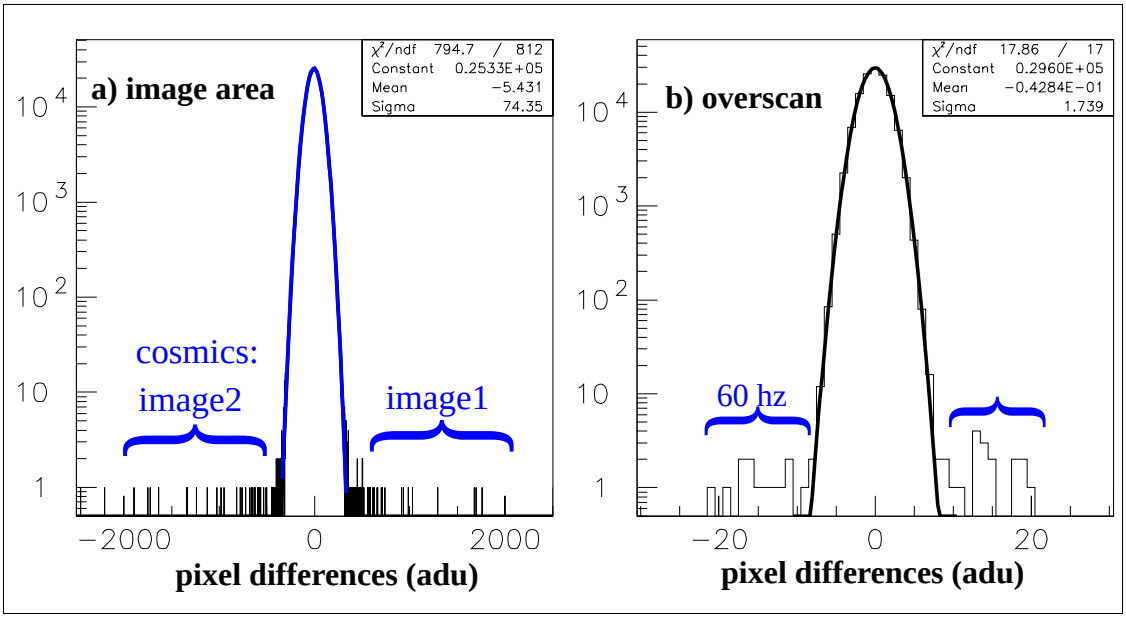

Figure 7: **a)** pixel{image 1} - pixel{image 2} (cosmics outliers); **b)** same for overscan area (60hz noise outliers)

charges generated in one of the two images by ionizing radiation. On the other hand the overscan is exactly fitted by a gaussian representing the electronic gaussian noise with a few outliers at 60hz. The gaussian noise in the image area is mainly photon statistic noise but not only. Therefore if we apply the ordinary formula giving the electronic gain constant k_e we overestimate the number of electrons and the quantum efficiency. Moreover we have not taken into account the fact that the mean number of electron and therefore its dispersion depends on the pixel considered. Technically we include this dependence by making a regression analysis of the distribution of the difference of a given pixel count in image-A and in image-B versus their sum. Figure 8 displays surprisingly little dispersion of what ought to be the number of photon inpinging the half CCD times the quantum efficiency.

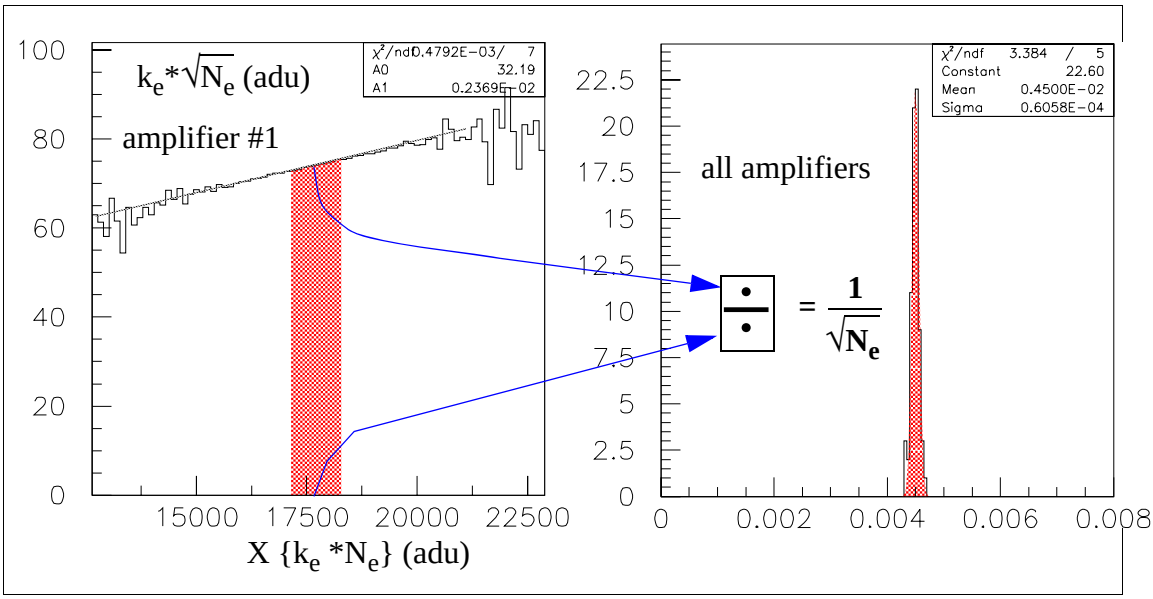

Figure 8: **left :** for each X slice (128 adu) the RMS of the histogram of pixel(A)-pixel(B) gives Y and regression analysis gives Y=a*X+b (the fitted slope is compatible with the square root function) ; **right :** Y is computed at the center X_C of the pixel gaussian distribution (Figure 5a) and the ratio $Y(X_C) / X_C$ is histogrammed.

2.5 Electronic model of Megacam

The characteristic features of the Megacam electronics are seen in Figure 9. It consists

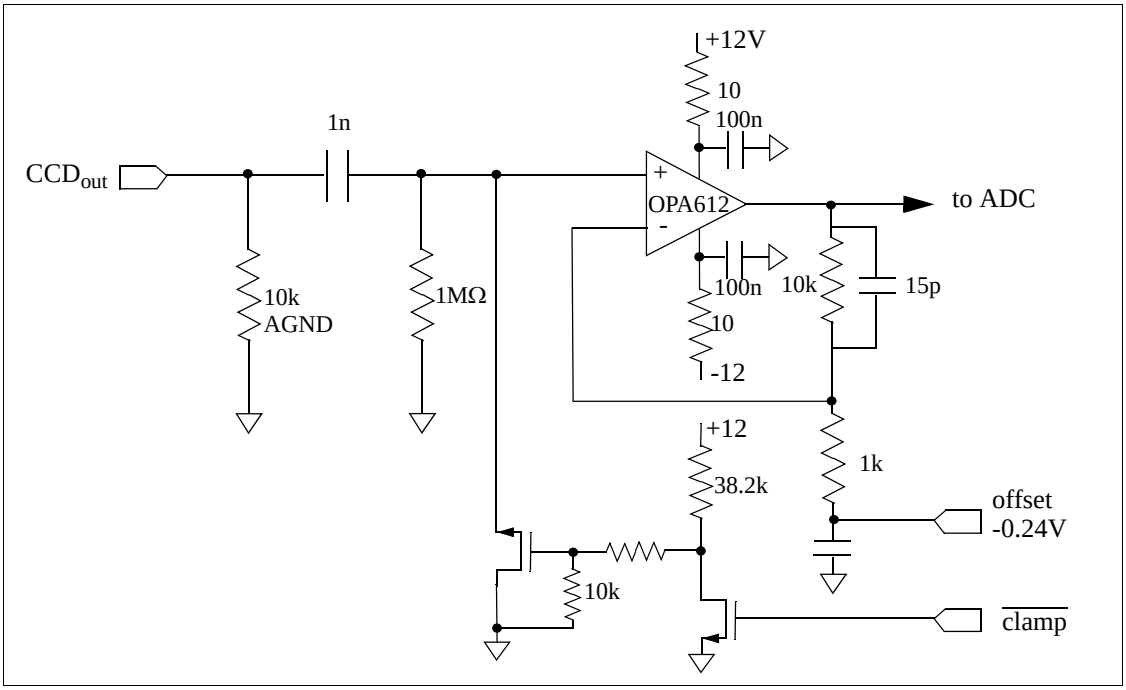

Figure 9: Schematics of Megacam Clamp and Sample CCD readout

in freezing the DC level of the amplifier input (using the 'clamp' command) while the preamplifier input level (inside the CCD) is frozen in the reset state following the the

readout of pixel n-1. It is worth remembering that this CCD reset level is varying randomly due to so-called KT/C noise with an amplitude corresponding to a few hundreds e^- and that the CCD preamplifier output is not refered to ground. In a nutshell: clamping has two functions -DC restore and KTC noise suppression-. In a report (LPNHE 2004-11), we have shown that this method has only advantages compared to others[2]. In particular we have demonstrated and checked experimentally that the clamping noise is 0.5 e^- only. This digitization method could be made exceptionally robust with amplitude measurement depending only on the timing of one clock (convert) and not at first order. However the features observed on SNDICE flat field images (§3.2) and the behaviour of overscan data (§2.2 and §2.3) might be related with megacam peculiar clocking scheme[3].

3 Testing the Uniformity and Reproducibility of SNDICE-Megacam images

3.1 Analysis of contrast found in Sndice-Megacam images

3.1.1 small scale effects

It is known from test bench studies that the uniformity of the Sndice light field inside the megacam aperture is characterized by a RMS contrast smaller than 0.5%. In the much smaller aperture covered by one CCD amplifier, the RMS contrast is expected to be below 0.1% (added quadratically to the photon noise, which is 0.4% as seen on Figure 5-b). Actually as seen earlier in Figure 5 the RMS contrast is much larger (~4%) and rather uniform. In order to visualize how the diffractive scattering yields this contrast we put in Figure 10 an image of the quarter of a CCD amplifier using a black-to-white grey scale covering the interval [-1.5 σ ,+1.5 σ] around the average level. A closer look shows that in 'normal' superpixels C and D the effect of darker and brighter rings are averaged out by projection leaving a low X frequency variation and a high X frequency noise both of the order of one per mil. In B and E we see that the effect of dark rings is visible in projection as a 1.5% dip. The projection act as a low pass filter in one dimension which reduces the 4% diffractive noise to less than a percent. But it reveals also non diffractive absorbing effects such as the deep (3%) dark spot in the upper left of A, or a shallower one in C.

3.1.2 large scale effects

We get a large scale picture of megacam in Figure 11. The features which do not enter in the description of the previous paragraph are circled. The dark spot on amplifier #21 yields an accumulation (a 'shoulder') in the dark side of the distribution as seen on

[2] Historically correlated double sampling scheme was introduced for suppressing low frequency system noise (60hz). For megacam pickup immunity comes from the proximity of detector and electronics within a common shield

[3] the few per mil precision obtained is well within megacam specifications but it falls short of the 10^{-4} precision convenient for the present sndice analysis

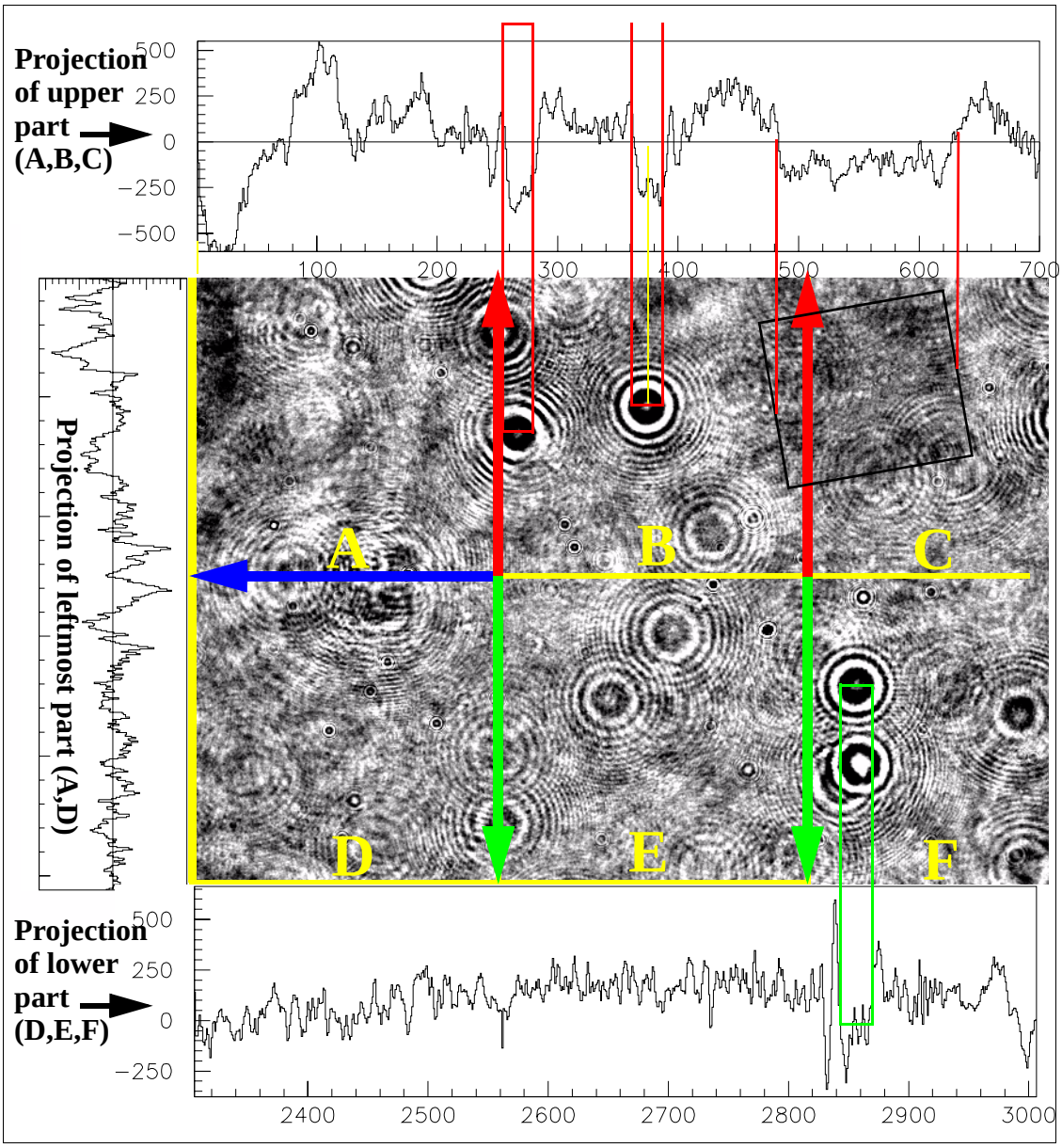

Figure 10: The underlying megacam image is drawn pixel by pixel with a grey scale around the average level (black=<-5%; white >+5%). 'Superpixels' (512*512 pixels) are labeled A to F. The A-B-C and D-E-F superlines projection on X axis are seen on top and bottom sides and the A-D supercolumn projection is seen on left side. The effect of dark round spots X projections is seen in B and F. A rectangular shade is also seen in top left part of C.

Figure 12 (left). The same shoulder is seen in amplifier #24 and to a less extend in amplifiers #16 and #20. In amplifier #53 and #54 there are both a dark and a bright shoulder of smaller amplitude. This well understood by looking at the dark and bright rings of a different type. The optical defects causing the rings are often attributed to dust. We reject this hypothesis at least when the rings are aligned across the whole field (for example along the white straight line in Figure 11). At last the distribution of amplifier #28, also shown in Figure 12 (right), presents a small bright side excess due to the reflexion image of the focal plane on the field corrector lens which yields bright filements superimposed to the normal picture.

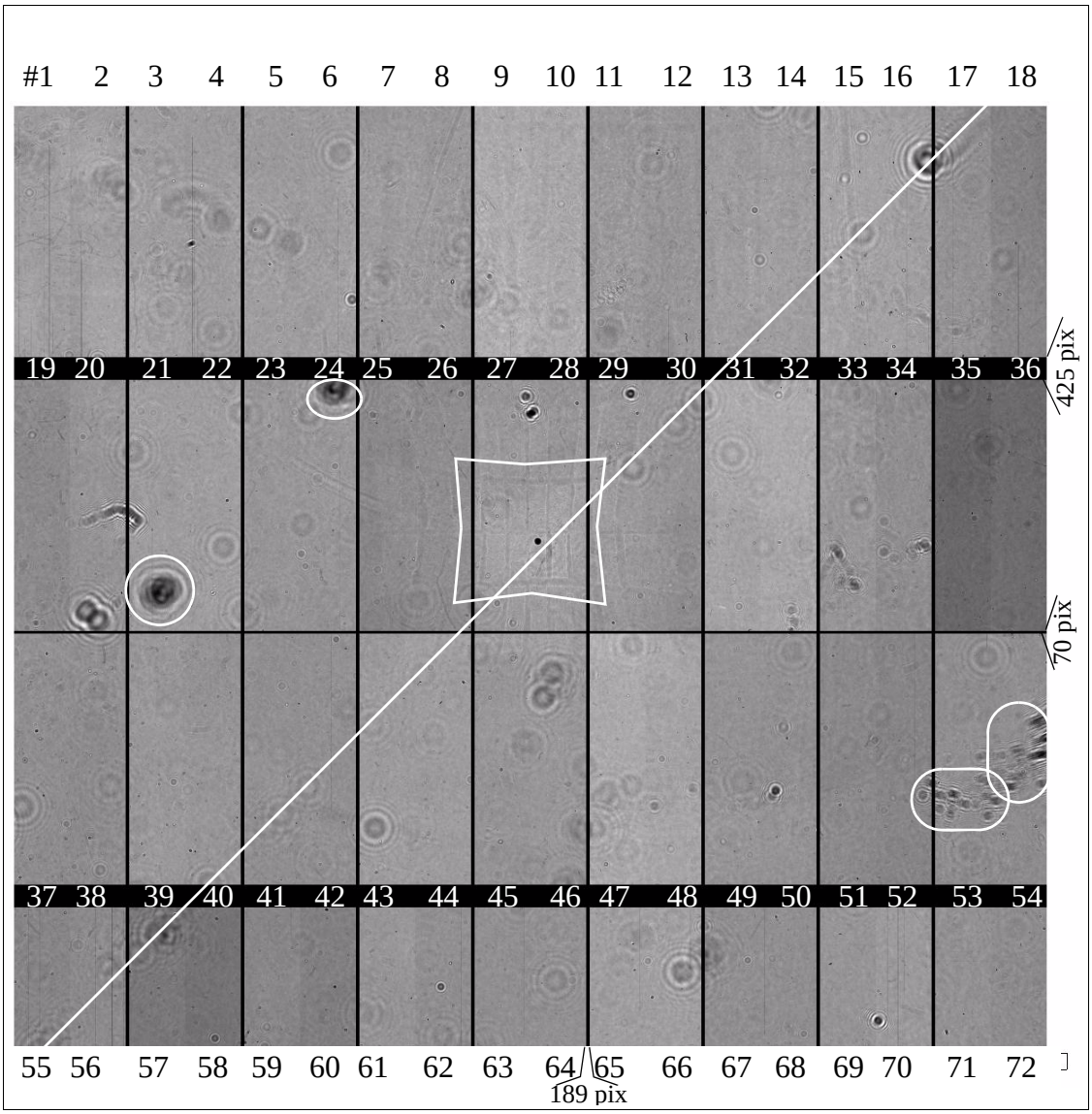

Figure 11: General view of megacam's focal plane as a mosaic of 72 amplifier (#1 to 72) realized with one of the 25 images with identical sndice illumination. Features yielding non-standard distribution at the amplifier level are circled. The line traversing the field diagonnally guide the eye to follow the alignment of optical defects

We should remark that the field calibration process described in §2.4 is not affected by any of the defects presented here. Moreover SNDICE detects optical defects which are not accessible by other methods. It yields the tools allowing to design and maintain a catalog of defects and to mitigate their effect.

3.2 Short timescale Fluctuations of Megacam images

When comparing sndice-megacam images taken at one minute intervals we find a rather paradoxical situation. First the pixel distribution is essentially gaussian as predicted for perfectly reproducible images with Poisson photon noise seen in Figure 7-a, but if we subtract the two images and visualize the result we discover many patterns which give a

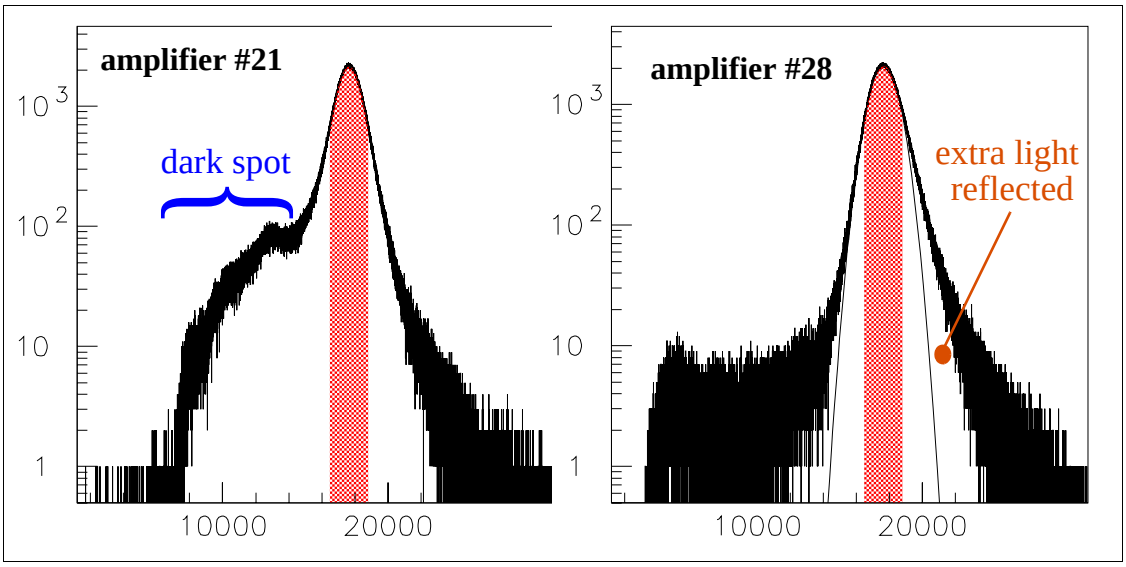

Figure 12: the skewed distribution of pixel counts within amplifiers #21 and #28 is related to their defects identified in Figure 11

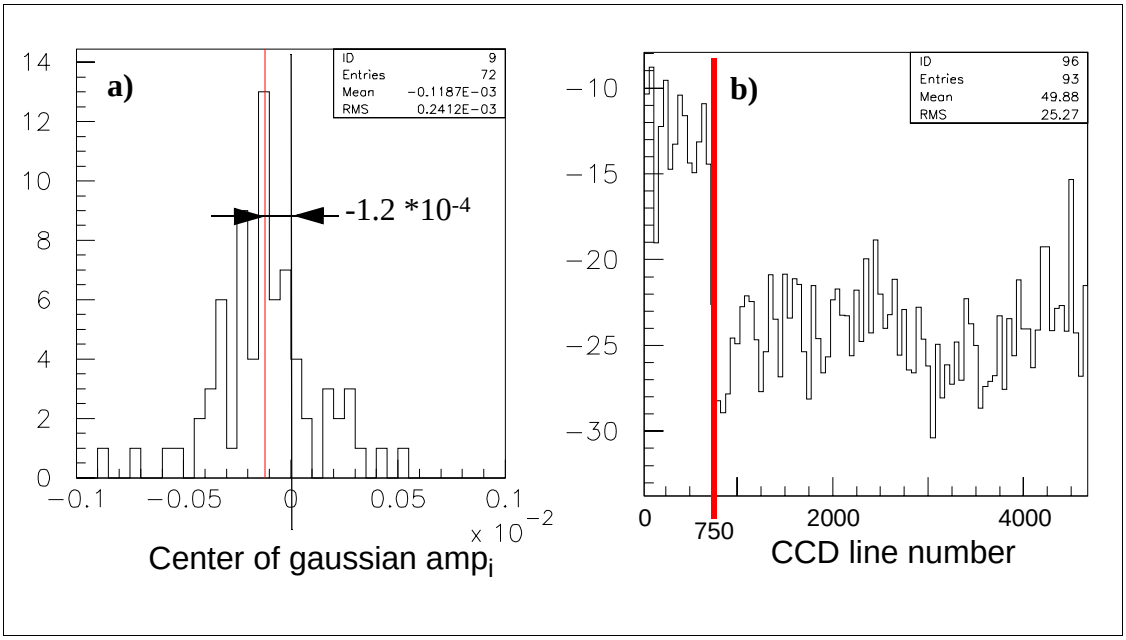

Figure 13: **a)** Individual fluctuations of each amplifier between two images taken in sequence (center of gaussian difference). The 72 amps average is smalll and well included in Figure 6-b
b) The difference of the total CCD content for two consecutive identical images as a function of the line number shows a break at line #750 can be interpreted as a 0.16% variation of the gain during the readout of the image

signature for different sources of non reproducibility either from megacam electronics or from optical transmission effects. Moreover the gaussian difference of two images is not centered on zero. The general behaviour of the central value averaged on the 72 amplifiers of the whole megacam, as discussed earlier in Figure 6, is compatible with a simple global temperature effect affecting the gain. But Figure 13-a shows that it hides a more complicated situation: the gain of one amplifier varies more that the average of

the 72 amplifiers (in some cases by 0.5 or even 1 per mil between two exposures). Figure 13-b shows that this variation of gain can be rapid enough to appear during the readout of an image in the short time (few miliseconds) needed to read a few lines. To make it more complicated some irreproducibilities of the same magnitude due to optical transmission variation seem to be mixed with these electronic effects. The whole focal plane image obtained as a difference of two whole images, as seen in Figure 14, displays

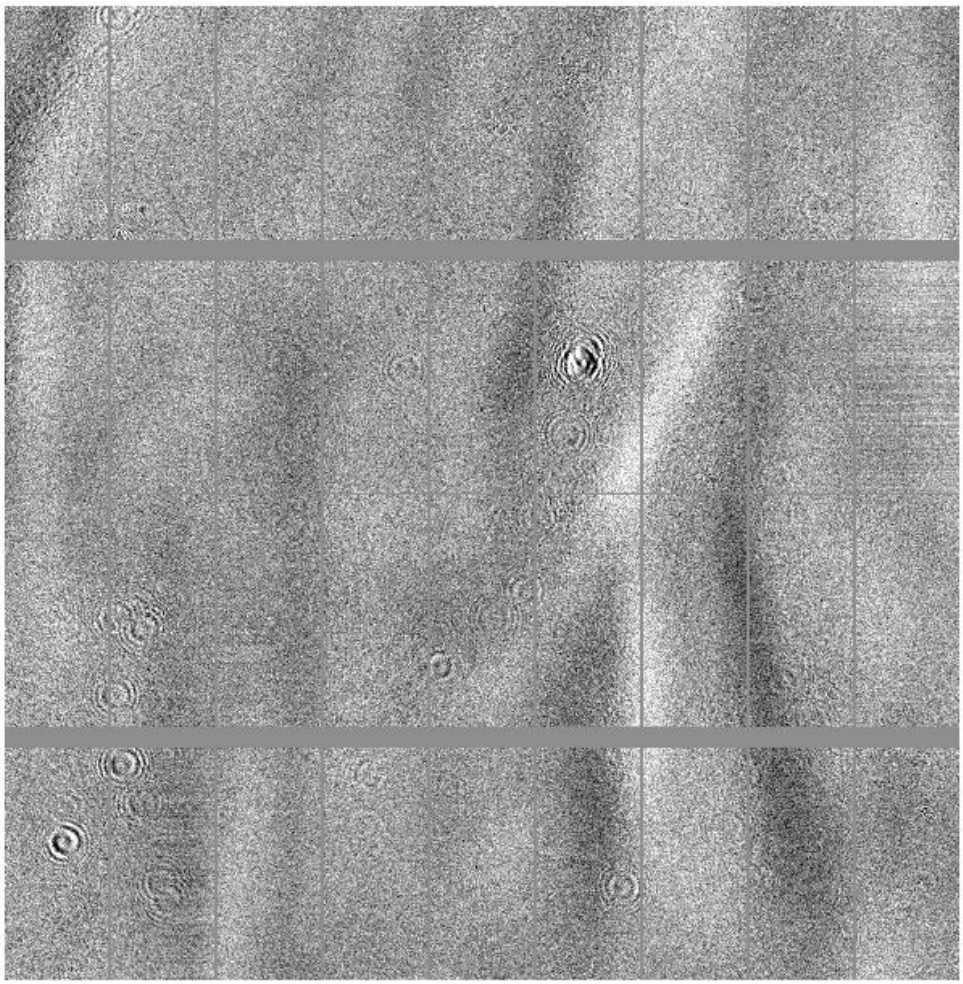

Figure 14: This Megacam image is made by a pixel to pixel subtraction of two consecutive images obtained with identical SNDICE illumination

either large scale effects not depending on amplifiers boundaries or small scale effects related to diffractive rings. The former are rather mysterious and the latter could be due to a displacement of the surface carrying an optical defect or to the displacement of the line of sight. Non reproducibilities will be studied more precisely in Section 3.5 using various spatial filtering techniques.

3.3 Determination of the absolute electronic gain using photon noise

We have sketched in Section 2.4 the use of the classical electronic calibration method based on photon statistics. Under its basic assumptions -essentially the reproducibility of the light flux and of the optoelectronic response (digitization included)-, we have shown that the large number of pixels per amplifier ($4.6*10^{-6}$) yields a very precise electronic calibration of each amplifier. In particular the non uniformity of the image is dealt with the slicing of the ADC distribution of a pixel (128 adu/slice). In each slice the distribution of the difference of pixel contents is gaussian and we fit independantly its mean and sigma (cf. Figure 8).

We have shown is the previous paragraph that the reproducibility hypothesis is wrong, or at least insufficient : the difference between the expected value of the same pixels of successive images beeing in certain cases equal or bigger than the photon noise RMS (~70 adu).

The aim of this paragraph is to show how we overcome this problem by using four spatial frequency halving operators :

$\Sigma_x : (f_{i,j} , f_{i+1,j}) \rightarrow (f_{i,j} + f_{i+1,j})/2$; $\Delta_x : (f_{i,j} , f_{i+1,j}) \rightarrow (f_{i,j} - f_{i+1,j})/2$

$\Sigma_y : (f_{i,j} , f_{i,j+1}) \rightarrow (f_{i,j} + f_{i,j+1})/2$; $\Delta_y : (f_{i,j} , f_{i,j+1}) \rightarrow (f_{i,j} - f_{i,j+1})/2$

The matrix element $f_{i,j}$ is the expected value of the content of the pixel in column i and line j. It can be considered as a discrete time sampling of the continuous «contrast» function f(x,y) at the node (x_i, y_j) of a rectangular network. The sampling of $f_{i,j}$ is governed by Poisson statistics of N photons. It is approximated by a gaussian law of mean value $f_{i,j}= \alpha N$ and width $\sigma_{i,j}= \alpha\sqrt{N}$. The non reproductibility of the sndice-megacam imaging can be represented by an auxiliary random «discrepancy» function $\delta f(x,y)$ which expected value on a sequence of «identical» images is null.

The role of the derivative operators in this problem is to yield derivative images with a much reduced contrast as compared with the original images. The ultimate hope is to be able to neglect the derivative of the discrepancy in comparison with the Poisson noise.

Practically the derivative operators Δ are part of a (Σ, Δ) doublet which creates a reversible operation yielding two images while halving the number of lines (or columns). In order to conserve an x*y symmetry we use the product $(\Sigma, \Delta)_x \times (\Sigma, \Delta)_y$. Each image yields four images with half the number of lines and half the number of columns, namely: $\Sigma_x \times \Sigma_y$; $\Delta_x \times \Sigma_y$; $\Sigma_x \times \Delta_y$; $\Delta_x \times \Delta_y$. Each pair of consecutive images yields 8 images, respectively the four sums and the four differences of the four previous ones (cf.Figure 15). The essential point for the analysis of photo-electron statistics is the fact that each corresponding pixels in these eight images follow the same Poisson statistics[4]. We can test that hypothesis using three criteria:

- **A-** the gaussiannity of the pixel difference distribution for each amplifier and each slice
- **B-** the nullity of the mean value of gaussians
- **C-** the evolution of the width of the gaussians as a $\sqrt{N}$ function of the slice (N is the average number of photo-electron per pixel in a given slice)

[4] they are linear combinations of 8 gaussian variables differing only by the sign of the coefficients

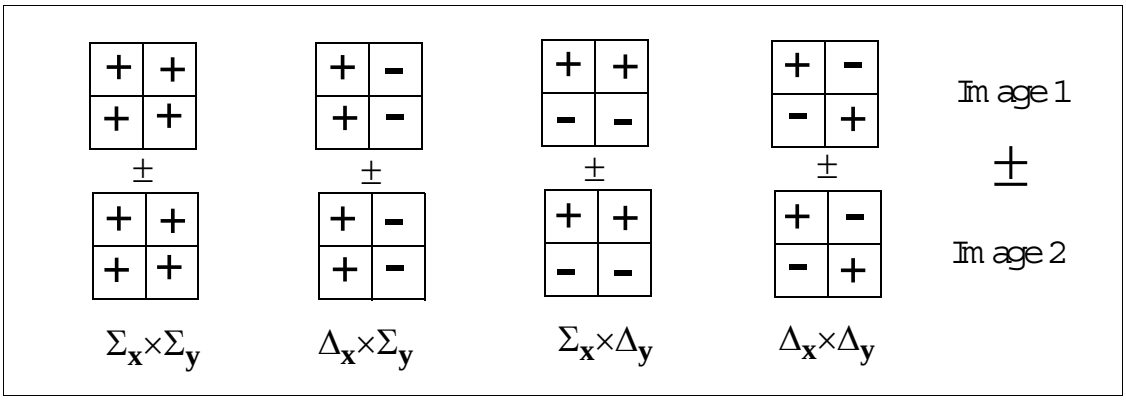

Figure 15: Four filters acting on every pair of adjacent pixel lines (or columns) with coefficients +1/4 or -1/4 (the figure indicates the respective pattern of these coefficients); Filtering image1 provides four derived images respectively added or subtracted to those derived from image2

The first two criteria are visualized in Figure 16 and the third in Figure 17-a.

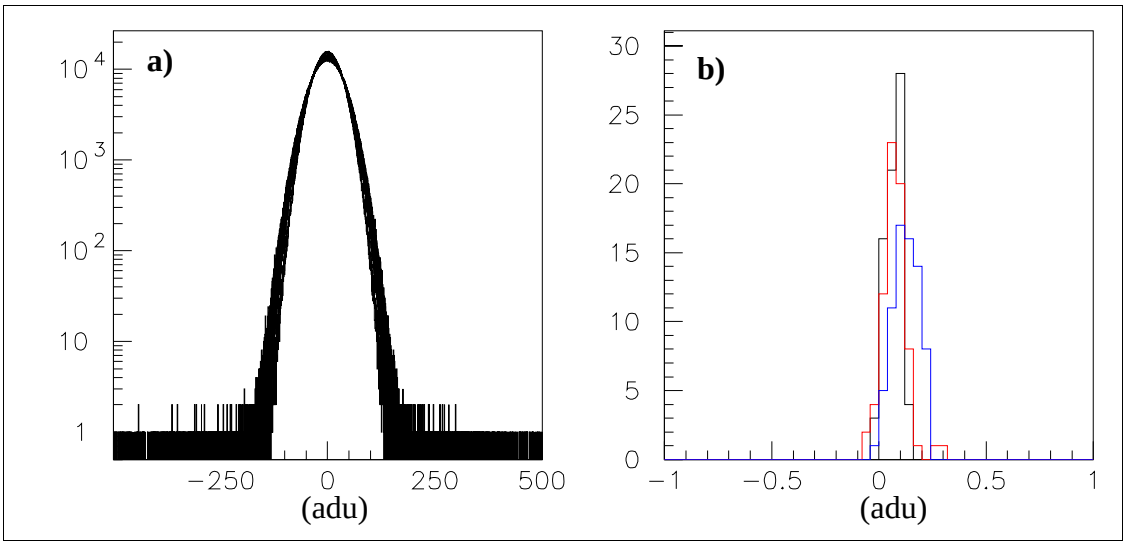

Figure 16: **a)** Gaussian test (**criterion A**) : The distributions of the difference of pixel contents between two consecutive «$\Delta_x \times \Delta_y$ images» (72 gaussians are overdrawn -one per amplifier).
b) Nullity test (**criterion B**) : in black the distribution of mean values of these 72 $\Delta_x \times \Delta_y$ gaussians (blue and red : the same for $\Delta_x \times \Sigma_y$ and $\Sigma_x \times \Delta_y$)

We consider that among the four images produced by the four operator introduced above, three pass the test. They are the three images obtained with derivative operators ($\Delta_x \times \Sigma_y$; $\Sigma_x \times \Delta_y$; $\Delta_x \times \Delta_y$). The fourth one ($\Sigma_x \times \Sigma_y$) is just the original image with a resolution reduced by a factor two. In summary we have 5 estimates for the electronic calibration factor of an amplifier, three of them being demonstrably better. We have a reason to expect that the doubly differential operator ($\Delta_x \times \Delta_y$) is better than the others : it yields a contrast RMS smaller. The study of gain variations suggests also that it mitigates the effect of different electronic gain unstabilities. The optimality of $\Delta_x \times \Delta_y$ can be checked rigorously by showing that the width of its distribution is minimal. For this purpose Figure 17-b plots for each amplifier the difference between the width of a given estimator and the minimal one. The intuitive explanation is that the non-Poisson noise is

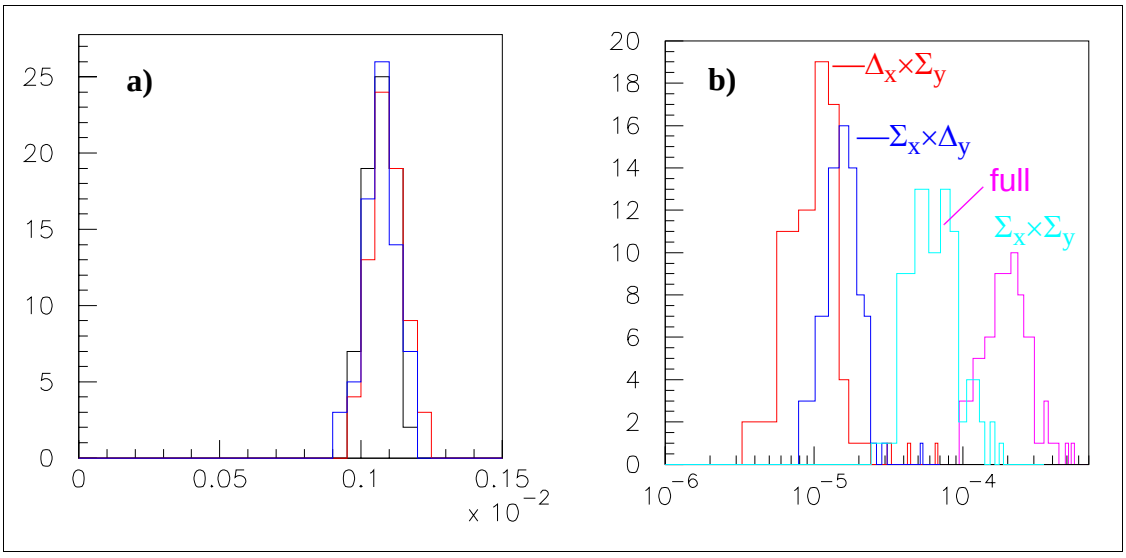

Figure 17: a) Criterion C :Distributions of the derivative of the gaussian width as a function of the charge collected in a pixel for the three "good" operators (— $\Delta_x \times \Delta_y$; —$\Delta_x \times \Sigma_y$ and —$\Sigma_x \times \Delta_y$) applied to the 72 preamplifiers
b) The positive value of the excess RMS width drawn here $\sigma(\Delta_x \times \Sigma_y) - \sigma(\Delta_x \times \Delta_y)$; $s(\Sigma_x \times \Delta_y) - \sigma(\Delta_x \times \Delta_y)$; $\sigma(\Sigma_x \times \Sigma_y) - \sigma(\Delta_x \times \Delta_y)$; $\sigma(\text{full}^a) - \sigma(\Delta_x \times \Delta_y)$ confirms that $\Delta_x \times \Delta_y$ is the best Poisson noise estimator
a. the full image estimate of Figure 8 right. A pixel ratio 1 to 4 yield an extra calibration factor 1/2

correlated along a CCD line, or independently along a column. Therefore our three best operators suppress either line noise, or column noise, or both.
The conclusion of this study is logically to replace all the estimators of electronic calibration by the best one produced by the $\Delta_x \times \Delta_y$ filter. We shall have a look at the improved quantum efficiency estimate using the method of Section 2.4. We recall that the quantum efficiencies of the whole focal plane are surprisingly little dispersed. However a good consistency check consists in comparing the difference between the quantum efficiency of both halves of a given CCD to the average difference from one CCD to the next. The regression analysis in Figure 18 shows that the RMS difference of QE measured within the two halves of a same CCD is 0.3% while the RMS dispersion of QE within the lot of 36 CCDs is 1.5%. The main advantage of this measurement is to calibrate the gain of the electronic chain independently of the light flux and the quantum efficiency of the CCD. Its drawback is to be less sensitive than the estimators based on a pixel count average which depend on the product of the gain, the flux transmission/ reflection and the CCD quantum efficiency.

3.4 Study of the stability of the absolute electronic gain

In the previous paragraph, by comparing two images taken at one minute interval, we determined the absolute gain of each CCD digization chain (i.e. the number of adu per photoelectron) independently of local variations of flux and quantum efficiency. We checked that the dispersion of electronic gain (≤20%) is larger that the dispersion of flux or efficiency. Thus gain corrected SNDICE images, after smoothing interference rings, are rather uniform. Their residual non uniformity is essentially due to a 1.5% rms

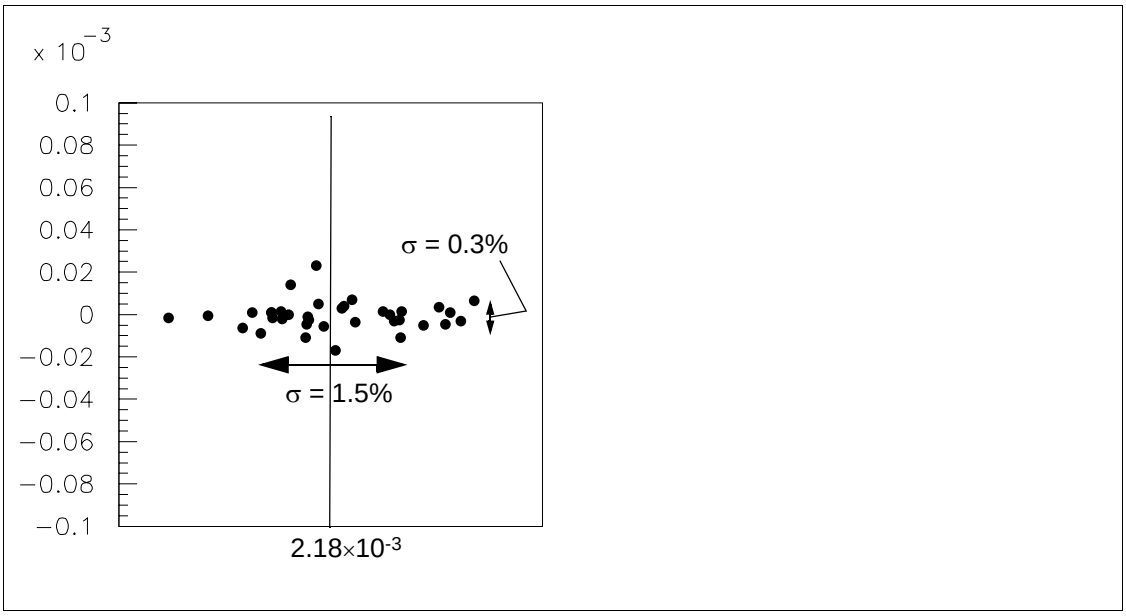

Figure 18: The difference (0.3% RMS) versus the sum (1.5% RMS) of two quantum efficiency indicators measured within the same CCD by its two independent readout chains. This difference (0.3%x2.18%) is not much larger than the $N^{-1/2}$ precision reached by estimators based on Poisson statistics for all photons ($N=10^{11}$) counted by a given amplifier.

difference of quantum efficiency from one CCD to the next (cf. Figure 18). The difference of integrated SNDICE yield for the two halves of a given CCD read through two different digitization chains are only 0.3%. The three components of this yield are flux, efficiency and gain. The differential operator method exposed in previous paragraph turn off local variation of flux and gain, thus the observed fluctuations of differential pixel photoelectron content are just depending on the total number of electron in a pixel and eventually on the average gain for each amplifier and for each image. We compared the 24 pair of images receiving almost identical integrated fluxes (at the $2*10^{-4}$ level as seen in Figure 6). The comparison proves that the CCD gain fluctuates randomly within a few parts per mil from from one image to the next and independently for the 72 amplifiers although the average of all amplifiers is stable (cf.Figure 19).

However the precision depends on the square root of electron number, not on the number of electrons as in a flux measurement. This yields a 0.15% precision when using all the $4.6x10^6$ pixels seen by a single preamplifier which is not sufficient to understand the behaviour of the electronics. Moreover the meaning of an effective electronic gain determined using two images with different individual gains is not clear! (sum and difference).

3.5 Discriminating effects affecting the reproducibility of Megacam images

while the precision of the flux falling on a single CCD line (one out of 4,600 in the same region) reaches 0.015%.

The study of the gain fluctuations at a smaller scale (such as the superline or the supercolumn scale) shows even larger fluctuations .

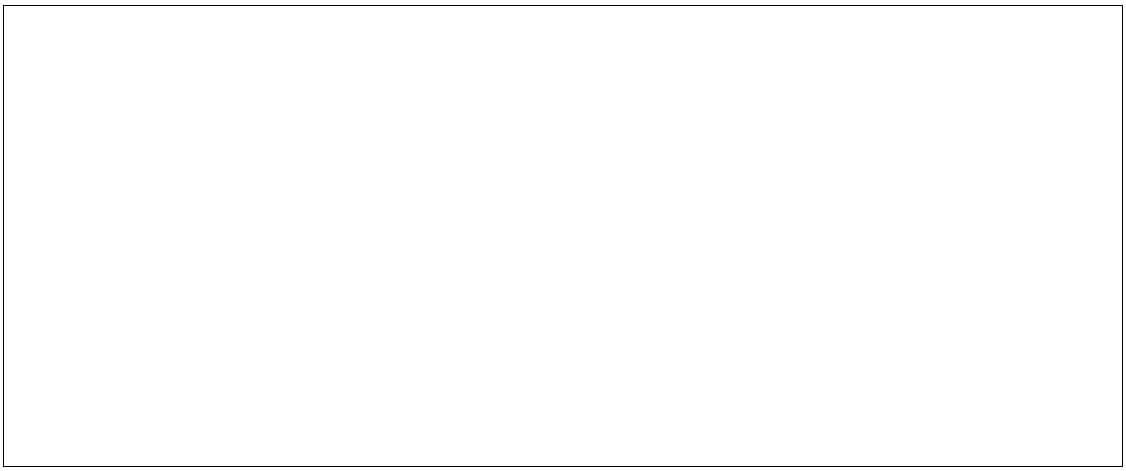

Figure 19: Fluctuation of the electronic gain during the 25 images run

by subtracting projected line or column profiles such as those seen in Figure 10. A 10^{-4} instability affecting only one line or one quarter of a column would create a one σ effect (which corresponds the square root of the number of the 10^{-8} photo-electrons created in 1024 pixels).

3.6 conclusion temporaire

{reste a expliquer les instabilités}

Le résultat principal est que l'on peut faire une étude complète de la réponse CFH+Megacam avec une seule incidence et deux images successives à flux moyen.
Cette étude fournit quatre données indépendantes:
1) l'e2u (electrons par Uadc) constante de calibration electronique.
2) la flucacité (produit flux de photons- efficacité_quantique).
3) la texture des micro défauts (taux de modulation due à la diffusion à petit angle).
4) la carte des taches (absorption et diffusion à grand angle)
Les algorithmes pour obtenir les 3 premières données sont simples et au point. Le quatrième peut utiliser un outil de base simple (les projections en superbandes X et Y), mais la notion de catalogue de défauts et de reflets 3d reste à établir en utilisant de la stereo (défauts classés par taille et section efficace décroissantes, reflets par brillance).
Les 3 algorithmes sont robustes -insensibles au premier ordre à la présence de taches ou de reflets- et de plus l'effet des taches est localisé en quatre taches principales affectant une dizaine de superpixels sur un total de 648 (même en doublant le nombre de taches cela reste manageable).
Un problème technique abordé par Kyan mérite d'être clarifié, c'est la carte du pedestal sur chaque CCD. Elle s'obtient par rampe de flux obtenue de préférence par variation du courant LED à durée de pulse fixe et non par durée d'obturation mécanique (qui donne le t0 de l'obturateur). On obtient en même temps la linéarité du flux LED à comparer avec la calibration sur banc. La variation d'obturation électronique est à faire après correction du firmware backend LED. Cependant on n'attend pas de grosse différence par rapport au pedestal utilisé dans l'algorithme actuel -le niveau double-overscan-.

Ces considérations éliminent le besoin de faire des séries d'images à des incidences différentes pour faire une médiane, ce qui en pratique ne fait que faire valser les petites taches. Plus exactement cela permet d'aborder de nouveaux problèmes avec des comparaisons d'incidence comme la qualité du miroir, la réflectivité en fonction de l'incidence et le mapping des défauts de l'optique proche du plan focal.
Il faut établir une stratégie de monitoring du genre:
1) stabilité de l'e2u : dérive (échauffement électronique Megacam), ou bruit conservant une bonne stabilité moyenne à court terme de l'e2u, ou encore reproductibilité à long terme (d'un an sur l'autre). Autant de mesures de l'e2u que de couples d'images successives a obturation électronique. Sur une séquence de 25 images on peut distinguer la dérive de l'électronique (e2u) de celle de la LED (flucacité).
2) optimisation de la mesure de flucacité : comparer la mesure globale qui semble assez précise pour définir des efficacité moyennes par superpixels (le filtrage des taches étant assuré par la troncation des distributions des histos de pixels) la continuité du flux étant assurée par le lissage des superpixels et la mesure locale (filtrage assuré par troncation des taches et filtrage des hautes fréquences spatiales) la continuité étant assurée par le lissage des flucacités projetées par superbandes.
3) étude de la stabilité de la flucacité : les indications actuelles de l'analyse locale font apparaitre une non-reproductibilité des flucacitées projetées dans une superbande d'une image à la suivante. En supposant l'efficacité quantique constante, il reste à comprendre les phénomènes exposés dans les Figure 13 et Figure 14. Flux ou électronique? Suivant les cas on peut espérer soit fixer des cartes d'efficacité quantique et monitorer les flux transmis et/ou les fluctuations locales de la réponse électronique (sans doute les supprimer par averaging).
La réponse ultime résiderait alors dans une procédure optimale pour mesurer les flux transmis (avec une résolution spatiale 1-15 mm) indépendamment des fluctuations de l'appareillage et dans la connaissance de la précision de cette procédure.
La notion de flat-field comme constante de calibration de flucacité qui serait fonction du numero de pixel (non-corrélée aux voisins) est naive et fausse, entre autre parceque le phénomène physique à étudier est le partage des photoélectrons entre pixels voisins et non la variation d'efficacité quantique sur la distance interpixel. Par contre les propriétés statistiques des facteurs de formes de pixels en fonction des lignes et des colonnes est significative (soit des masques de photolithographie, soit de la dynamique de collection des électrons). Des effets significatifs ont été mis en évidence par les statistiques des opérateurs integro-différentiels du §3.3. Cela vient du fait que nos flats ne sont pas plats. Les anneaux d'interférence contiennent des fréquences spatiales plus élevées que la résolution des pixels et invariantes par rotation (les différences d'acceptance entre lignes et colonnes voisines sont dont dues aux CCD et pas à l'illumination). L'analyse des facteurs de formes de pixels se fait donc globalement sur un CCD complet, l'autre méthode étant de former une étoile artificielle de dimensions inférieure à la taille d'un pixel et de la déplacer par pas d'une fraction de pixel le long des rangées.